



X-ray timing studies of the low-field magnetar CXOU J164710.2–455216

HONGJUN AN¹ AND ROBERT ARCHIBALD²

¹*Department of Astronomy and Space Science,
Chungbuk National University, Cheongju, 28644, Republic of Korea*

²*Department of Astronomy and Astrophysics,
University of Toronto, 50 St. George Street, Toronto, ON M5S 3H4, Canada*

ABSTRACT

We report results of X-ray timing analyses for the low-field magnetar CXOU J164710.2–455216 which exhibited multiple outbursts. We use data taken with *NICER*, *NuSTAR*, *Chandra*, and *Neil-Gehrels-Swift* telescopes between 2017 and 2018 when the source was in an active state. We perform semi-phase-coherent timing analyses to measure the spin parameters and a spin-inferred magnetic field strength (B_s) of the magnetar. Using a semi-phase-coherent method, we infer the magnetic field strengths to be $3 - 4 \times 10^{13}$ G at the observation period (\sim MJD 58000), and by comparing with previous frequency measurements (MJD 54000) a long-term average value of B_s is estimated to be $\approx 4 \times 10^{13}$ G. So this analysis may add CXOU J164710.2–455216 to the ranks of low-field magnetars. The inferred characteristic age (τ_c) is 1–2 Myr which is smaller than the age of Westerlund 1, so the magnetar’s association with the star cluster is still secure. For the low dipole field and the large age, recent multiple outbursts observed from the source are hard to explain unless it has strong magnetic multipole components. We also find timing anomalies around outburst epochs, which suggests that there may be spin-down torque applied to the magnetar near the epochs as was proposed in magnetar models.

Keywords: pulsars: individual (CXOU J164710.2–455216) – stars: magnetars – stars: neutron – X-rays: bursts

1. INTRODUCTION

Magnetars are neutron stars with strong magnetic field typically greater than 10^{14} G (Thompson & Duncan 1995, 1996). They emit almost exclusively in the X-ray band and so are observed in that band as pulsating sources. Their rotation periods are in the relatively narrow range of 2–12 sec, and the spin-inferred dipole magnetic-field strengths at the surface $B_s \equiv 3.2 \times 10^{19} \sqrt{P\dot{P}}$ are greater than 10^{14} G for most magnetars (see Olausen & Kaspi 2014, for more details).¹ Note that the dipole formula is only representative because \dot{P} for magnetars is highly variable perhaps due to dynamical behavior of field lines.

X-ray luminosity of many magnetars is greater than their spin-down power, and they sometimes exhibit an

outburst, a sudden increase in flux by orders of magnitudes (see Mereghetti et al. 2015; Kaspi & Beloborodov 2017, for reference). In addition, X-ray spectra of some magnetars show a turn-up at ~ 10 keV (e.g., Kuiper et al. 2006). As these are not often observed in conventional rotation-powered pulsars (RPPs) with typical $10^{12} - 10^{13}$ G fields, it was suggested that the strong magnetic field of magnetars should play important roles inside (e.g., Perna & Pons 2011; Pons & Rea 2012) or outside the star (e.g., Thompson et al. 2002; Beloborodov 2013) to give magnetars the observational properties.

However, discovery of low-field magnetars (e.g., SGR 0418+5729 and Swift J1822.3–1606; Rea et al. 2010; Scholz et al. 2014) and RPPs with outbursts (e.g., PSR J1846–0258 and PSR J1119–6127; Gavril et al. 2008; Archibald et al. 2018) suggests that there should be other important factors (besides dipole magnetic fields) needed to explain the observational properties. Promising candidates are magnetic-multipole components (e.g., Perna & Pons 2011; Alpar et al. 2011;

Corresponding author: Hongjun An
hjan@cbnu.ac.kr

¹ See the online magnetar catalog for general properties:
<http://www.physics.mcgill.ca/~pulsar/magnetar/main.html>

Turolla et al. 2011; Carrasco et al. 2019); hints of these were found in some magnetars (SGR 0418+5729, 1E 1048.1–5937; Tiengo et al. 2013; An et al. 2014) where local magnetic loops were suggested based on possible cyclotron-line features in their spectra. Nevertheless, the dipole fields are still important, and it was suggested that outburst rates of magnetars depend sensitively on the dipole magnetic-field strength (for a given age and multipole strength) in magneto-thermal evolution models (e.g., Viganò et al. 2013). Therefore, accurately determining dipole magnetic-field strengths of magnetars with outbursts will be particularly useful to provide further inputs to the models, which can be done with precision timing analyses. Furthermore, measurements of timing properties of a magnetar in outburst can be used to test magnetar models with twisted fields (e.g., Thompson et al. 2002; Beloborodov 2009) which predict that timing properties of a magnetar may change before and after an outburst due to enhanced spin-down torque.

CXOU J164710.2–455216 (J1647 hereafter) is an old ($\tau_c \geq 400$ kyr) 10.6-s magnetar possibly associated with the massive star cluster Westerlund 1 (Muno et al. 2006). It exhibited multiple outbursts (e.g., Israel et al. 2007; An et al. 2013; Borghese et al. 2019), which makes this source particularly useful for studying outburst relaxation (e.g., An et al. 2018) and magneto-thermal evolution (e.g., Perna & Pons 2011; Viganò et al. 2013). However, the value of the spin-inferred dipolar magnetic-field strength of J1647 is controversial. A large value $\sim 10^{14}$ G was suggested based on data taken after 2006 and/or 2011 outbursts (Israel et al. 2007; Woods et al. 2011; Rodríguez Castillo et al. 2014), but An et al. (2013) inferred a time-average value of $B_s < 7 \times 10^{13}$ G with 90% confidence using the same data. While the inferred range of B_s is not very large, it is important to measure B_s accurately for this magnetar as it may be a low-field magnetar with multiple outbursts, contrary to what we expect in the standard evolutionary model (e.g., Perna & Pons 2011).

In this letter, we report our results of timing analyses for the possible low-field magnetar J1647 performed using X-ray data taken between 2017 and 2018 when the source was active. Spectral properties of the source during the time were previously reported in details (Borghese et al. 2019), so here we focus on timing analyses. We present our analysis results and compare them with previous ones in Section 2, and then discuss and conclude in Section 3.

2. OBSERVATIONAL DATA AND ANALYSIS

Table 1. Observational data used in this work

| Observatory | Obs. ids | $N_{\text{obs.}}$ | N_{pass}^a |
|---------------------------|-----------------------|-------------------|---------------------|
| <i>NICER</i> | 0020350101–1020350192 | 82 | 39 |
| <i>NuSTAR</i> | 80201050002, 4, 6, 8 | 4 | 4 |
| <i>Chandra</i> | 19135–8, 20976 | 5 | 5 |
| <i>Swift</i> ^b | 00030806064, 7, 8 | 3 | 2 |

^aNumber of observations which pass our criteria: $H > 25$ and net exposure > 200 s after removing flares (see text).

^bWindow-timing (WT) mode only.

2.1. Data reduction

We use X-ray data taken with *NICER* (Gendreau et al. 2012), *NuSTAR*, *Chandra*, and *Swift* observatories between 2017 and 2018 (Table 1). The *NICER*, *NuSTAR* and *Swift* data are processed with the pipeline software for each observatory integrated in HEASOFT 6.25, and the *Chandra* data are processed with `chandra_repro` of CIAO 4.10 along with the most recent calibration database. We use standard filters except for the *NuSTAR* data process for which we use strict filters to remove enhanced background near the South Atlantic Anomaly (SAA) passage (`saamode=optimized` and `tentacle=yes`); this turns out not to have significant impact on the results below.

2.2. X-ray timing analysis

For timing analyses, we barycenter-correct the arrival times using the *Chandra*-measured source position of R.A.=251.79242° and decl.=−45.871306°. We extract events from the imaging data using circular apertures of $R = 30''$ and $2''$ circles for *NuSTAR* and *Chandra*, respectively. It is very difficult to analyze *Swift*/PC data with a semi-phase-coherent method as noted by Borghese et al. (2019) because of the low timing resolution (2.5 s), small photon collecting area and short exposures. So we analyze the “window-timing” (WT) mode data only. We extract source events in the *Swift*/WT data using $20'' \times 100''$ boxes. We perform an initial timing analysis using the H test (de Jager et al. 1989) to set an optimal energy range for each instrument and find that 1.2–5 keV, 3–10 keV, 0.5–5 keV, and 1–10 keV bands are optimal for *NICER*, *NuSTAR*, *Chandra*, and *Swift* data, respectively. We use these energy ranges in analyses below but the results do not alter significantly if we change the energy bands slightly.

For timing analyses to estimate B , high-quality pulse profiles need to be constructed. However, during these observations the source is in an active state (Borghese et al. 2019), and there may be some low-level flares which can distort the pulse profiles. In addition some background flares may also be problematic if there is any. In particular, the *NICER* data are heavily con-

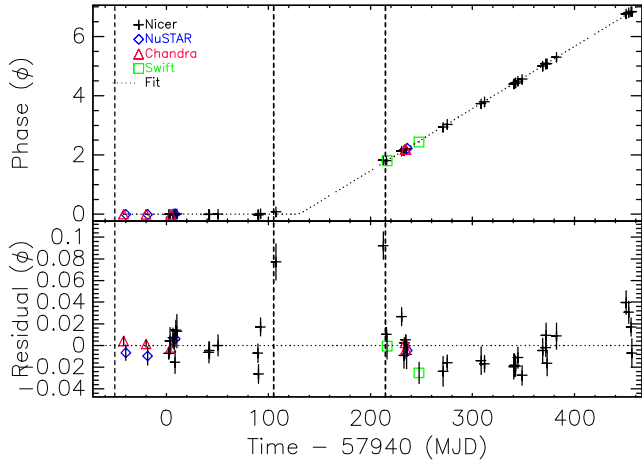


Figure 1. Timing behavior of J1647 during the observations. Epochs of outbursts are shown as vertical lines. Note that there is rotation ambiguity between data sets before and after MJD 58100, so the plot needs to be read with care. A frequency change and a quadratic trend in the later data are clearly visible.

taminated by flares but it is not clear whether or not these are from J1647; we do not find contemporaneous flares in overlapping data taken by the other instruments. Although the low-level flares from the magnetar can give us important information on the outburst relaxation of the source, here we focus on the persistent behavior. So we remove the flares whether or not they are from the source in order to measure the “persistent” pulse profiles accurately. We construct light curves with 1-s and 10-s time scales, search them for time bins which have larger counts ($> 3\sigma$) than the time-average value, and remove events in the time bins. We repeat this process until there is no more high-count bin in the light curves. There are very short flares ($\Delta t < 0.1$ s) in some *NICER* observations, and we also remove these. We then visually inspect the cleaned light curves and verify that there is no residual flare. This process removes a significant amount of the *NICER* exposures, and so unequal exposure among phase intervals and statistical fluctuation of background are concerns. So we further require that the H value for pulsation should be greater than 25 and the net exposure should be larger than 200 s (~ 20 rotations) in each observation. This removes 43 *NICER* and 1 *Swift* observations.

Next, we measure the spin periods in the earlier *Chandra* and *NuSTAR* data by searching for pulsations near the reported period of $P = 10.6106$ s using H tests. The pulsations are detected with high significance in these data, and we use these periods (e.g., $P = 10.6106(1)$ in *Chandra* Obs. ID 19135) as our starting point. We perform a semi-phase-coherent timing analysis by folding the data on the period. After iterating the analysis

a few times by adjusting the frequency (f) and its first time derivative (\dot{f}), the arrival phases align well until MJD 58047 when the phase jumps (Fig. 1). The phase jump may imply an anti-glitch, and so we check to see if f at this epoch is significantly lower than the model prediction (see below) using a H test but the data are insufficient to discern ($\sim 1\sigma$). In addition, the significance for pulsation is not very high ($H \sim 25$) and the pulse profile appears to be different from the others.

Nevertheless, we keep connecting the phases to the end of the data set, and the results are shown in Figure 1. The phases after MJD 58152 do not align with the previous ones and there may be arbitrary phase wraps, so the figure should be read with care; we make it to find frequencies to be used as starting points in analyses below. Although there may be phase wraps between the earlier and the later data, Figure 1 shows a clear quadratic trend in the later data (bottom). Since a single timing solution cannot be used throughout, we divide the data into two segments: before (seg. 1) and after (seg. 2) the gap.

We separately phase-connect the data in each segment and construct pulse-profile templates. For the templates, we use observations in which pulsations are detected with very high significance $H > 70$. The templates are fit with two asymmetric Lorentzian functions, and we reanalyze the data with the template functions (Fig. 2). The templates of segs. 1 and 2 differ slightly; the second peak is relatively larger and the separation between the peaks is smaller for seg. 1 than those in seg. 2; the separations of the peaks are $\Delta\phi = 0.195 \pm 0.008$ and 0.268 ± 0.009 for segs. 1 and 2, respectively.

We fold the data in each observation to produce a pulse profile, group the pulse profile to have at least 20 events per phase bin, and fit the profile with the template function by allowing the amplitudes and peak locations of the two Lorentzians and the background level to vary. Note that fitting both the locations and amplitudes of the peaks is very important because the pulse profiles may vary with time due to residual low-level flares (especially in the *NICER* data) and/or an intrinsic variabilities. For measuring arrival phases, we take the center position of the two peaks. We measure the arrival phases for all the observations in each segment, fit the phases with a quadratic function, and adjust f and \dot{f} to make the fit residuals flat; we find that higher time derivatives are unnecessary in either data segments. We update the profile template and shape parameters of the template functions, and then repeat the above process until no more change of f and \dot{f} is necessary. The final phase residuals are shown in Figure 2. Note that

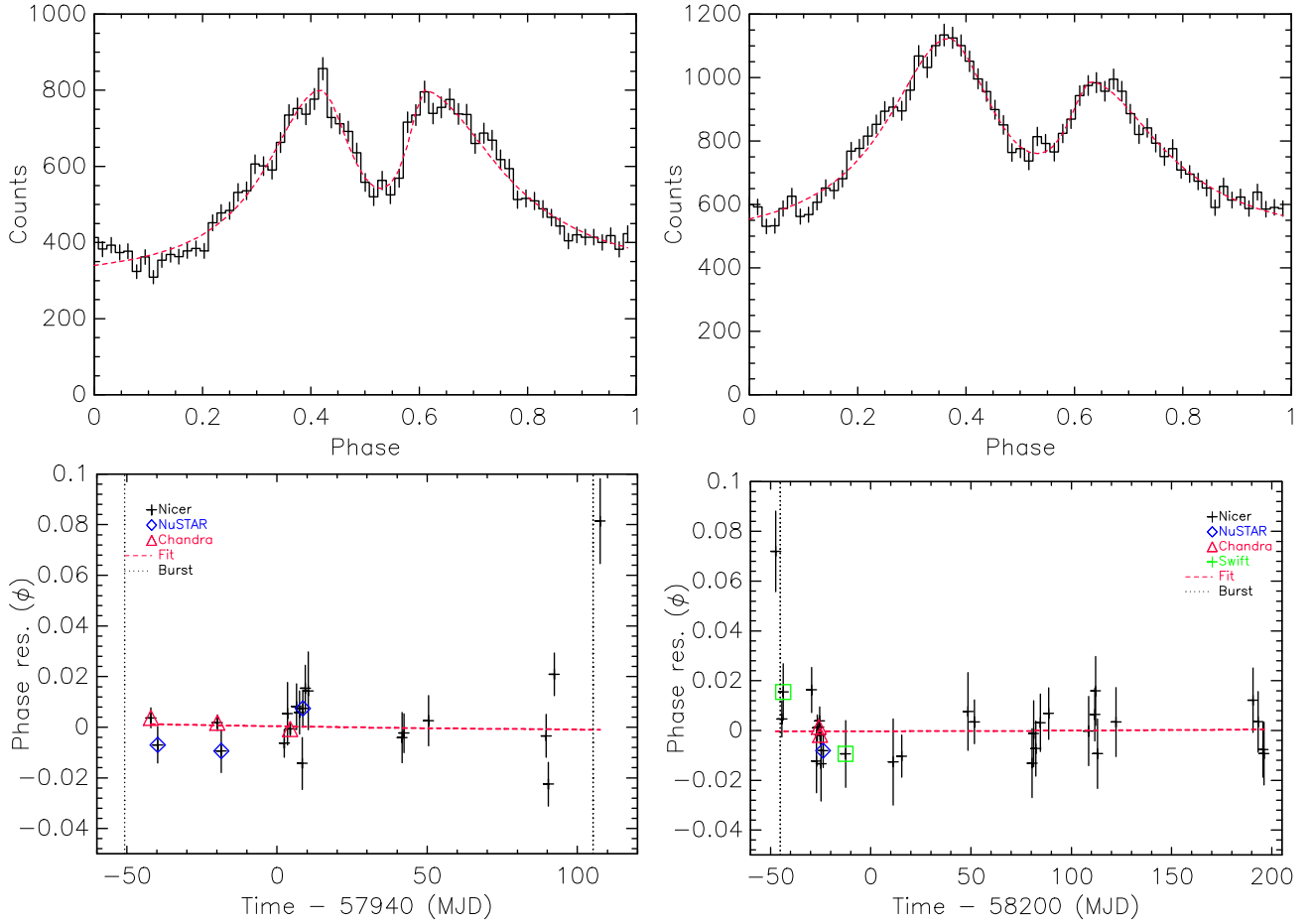


Figure 2. Pulse-profile templates and timing residuals for segs. 1 (2017) and 2 (2018). Figures in the left column are a pulse-profile template (top) and timing residuals (bottom) made with the *NICER*, *Chandra*, and *NuSTAR* data for seg. 1, and figures in the right column are a pulse-profile template and timing residuals for seg. 2. Best-fit functions are also shown in red dashed lines, and epochs of outbursts are shown in vertical lines. Note that the last point in the left panel and first three points in the right panel are excluded in the fit.

for the *Chandra* analysis, we added a systematic uncertainty corresponding to the timing resolution of 0.44 s for the subarray observations.

For the data in seg. 1 we measure the spin frequency and its first derivative to be $f = 0.0942445461(6) \text{ s}^{-1}$ and $\dot{f} = -6.4 \pm 1.9 \times 10^{-16} \text{ s}^{-2}$ ($\chi^2/\text{dof} = 26/17$), implying $B_s = 2.9 \pm 0.4 \times 10^{13} \text{ G}$ and $\tau_c = 2.3 \text{ Myr}$; the latter is smaller than the age of the Westerlund 1 cluster (3.5–5 Myr; Clark et al. 2005). The last data point in this segment is not used for deriving the timing solution even though the point is shown in Figure 2; including this point increases B_s to $3.5 \times 10^{13} \text{ G}$ but makes the fit significantly worse ($\chi^2/\text{dof} = 47/18$).

After an outburst in 2018 (MJD 58155; Borghese et al. 2019), timing properties of the source changed significantly; the frequency is smaller and $|\dot{f}|$ is significantly larger than those measured in seg. 1. In these data (seg. 2), the spin frequency and its first derivative are measured to be $f = 0.0942442962(7) \text{ s}^{-1}$ and

$\dot{f} = -1.37 \pm 0.08 \times 10^{-15} \text{ s}^{-2}$ ($\chi^2/\text{dof} = 15/25$), implying $B_s = 4.1 \pm 0.1 \times 10^{13} \text{ G}$ and $\tau_c = 1 \text{ Myr}$. The measured spin parameters are presented in Table 2. Note that we ignore the data points in MJD 58152–58157 around the outburst epoch in this analysis because they might have been affected by the outburst; when we include these points in the fit, B_s does not change significantly but the fit becomes worse ($\chi^2/\text{dof} = 34/28$).

2.3. Comparison with previous results

Although we are able to estimate B_s in the time period of 2017–2018, this estimation may be biased by the outburst activities and/or undetected long-term timing noise which might have changed the frequency derivative (e.g., Scholz et al. 2017). Then our estimation above may not be accurate, perhaps higher than the actual value if the measurements are affected by the radiative activities. However long-term \dot{f} estimated with frequency differencing might have been less affected by timing anomalies because of the long baseline (~ 11 years),

Table 2. Comparison with previous frequency measurements

| Epoch | f s^{-1} | \dot{f} 10^{-15} s^{-2} | B_s 10^{13} G | \dot{f}_{2017}^a 10^{-15} s^{-2} | $B_{s,2017}^a$ 10^{13} G | \dot{f}_{2018}^a 10^{-15} s^{-2} | $B_{s,2018}^a$ 10^{13} G | Ref. |
|---------|------------------------|--|------------------------------|---|---------------------------------------|---|---------------------------------------|---------------------|
| 53999.0 | 0.0942448896(18) | -8.2(6) | 10.0(2) | -1.009(5) | 3.51(1) | -1.651(5) | 4.494(7) | 1 |
| 53999.1 | 0.09424498(15) | >-3.6 | <7 | -1.3(4) | 4.0(7) | -1.9(4) | 4.8(5) | 2 |
| 53999.1 | 0.0942448814(4) | -8.633(9) | 10.277(5) | -0.987(2) | 3.474(4) | -1.631(2) | 4.467(3) | 3 |
| 54008.0 | 0.0942448774(11) | -7.4(2) | 9.5(1) | -0.975(4) | 3.454(7) | -1.620(4) | 4.452(5) | 4 |
| 54008.0 | 0.0942448813(14) | -11.4(9) | 11.8(5) | -0.987(4) | 3.474(8) | -1.631(3) | 4.467(6) | 4 |
| 57940.0 | 0.0942445461(6) | -0.6(2) | 2.9(4) | ... | ... | ... | ... | Seg. 1 of this work |
| 58160.0 | 0.09424442962(7) | -1.37(8) | 4.1(1) | ... | ... | ... | ... | Seg. 2 of this work |

Refs. [1] Israel et al. (2007), [2] An et al. (2013), [3] Rodríguez Castillo et al. (2014), [4] Woods et al. (2011).

^aTime-average \dot{f} and magnetic field strengths estimated by comparing with our segs. 1 (2017) and 2 (2018) results.

and so estimating a long-term averaged B_s using frequency differencing may provide an independent check. We do this by comparing our results with previous measurements made at the reference epoch MJD 54000 (Israel et al. 2007; Woods et al. 2011; An et al. 2013; Rodríguez Castillo et al. 2014).

In Table 2, we summarize previous spin-parameter measurements. While the previous measurements are all done near the same epoch, the results differ significantly because of different assumptions made in those works. However, the difference is small ($\Delta f \approx 10^{-7} \text{ s}^{-1}$), so errors in estimating $B_s \equiv 3.2 \times 10^{19} \sqrt{P\dot{P}}$ would not be large. Note that \dot{f} appears to have changed dramatically since the previous measurements which are probably affected by a putative glitch and its recovery in 2006 as noted by Woods et al. (2011) and An et al. (2013). This again justifies the time-differencing measurement. We compare the previous f values with our results and measure time-averaged \dot{f} to estimate time-averaged B_s for J1647. These values are shown in Table 2 and typically $B_s \approx 4 \times 10^{13} \text{ G}$.

3. DISCUSSION AND CONCLUSIONS

We analyzed X-ray data taken with *NICER*, *NuSTAR*, *Chandra* and *Neil-Gehrels-Swift* observatories in 2017–2018 to measure timing properties of the magnetar J1647. We found that the magnetar’s spin properties changed significantly after the outburst in 2018. We therefore split the data into two segments, and found that the magnetic field strengths were low $B_s \sim 3 \times 10^{13}$ and $\sim 4 \times 10^{13} \text{ G}$ in 2017 and 2018, respectively. While these values may be biased because of ‘undetected’ timing anomalies associated with the magnetar’s activities or timing noise, long-term time-averaged B_s which provides an independent estimation is also low $B_s \approx 4 \times 10^{13} \text{ G}$.

There were three major bursts in the data we analyzed (MJDs 57889, 58045, and 58155; Borghese et al. 2019). For the later two, the source was observed with *NICER* within ± 2 days and so measuring timing prop-

erties near the outbursts were possible although we ignored them when estimating B_s above. For the one measured at MJD 58047 (2 days after the activity), the sudden shift in phase, if real, may be due to an anti-glitch (e.g., Archibald et al. 2013). However a frequency measurement does not confirm this due to large uncertainty. Furthermore, the pulse profile at this epoch is distorted with one of the peaks not being clearly visible, which may be due to increased constant emission, contamination from low-level flares, or intrinsic (temporary) change of the profile. So the phase shift in this case is rather uncertain.

For the outburst at MJD 58155, a *NICER* observation was taken ~ 2 days ‘before’. For this, the pulse profile appears to be normal and the detection significance is very high ($H \approx 52$). So this shift seems to be real. *Swift* monitoring data (Borghese et al. 2019) do not cover the same period, so it is not clear whether or not this shift is associated with a spectral change. Nevertheless, the arrival time of the shifted pulse (~ 2 days ‘before’ the outburst) was later than expected from the rest of the data in the segment, which may imply that the star was spinning slower at the time (implying a glitch) although it is hard to tell conclusively without any measurement right before (i.e., a precise measurement of f). In the next observation at MJD 58156 the phase shift was recovered quickly (~ 1 day ‘after’ the outburst; Fig. 2) perhaps by an enhanced spin-up (i.e., glitch). Theoretically this may be explained by enhanced spin-down torque due to gradual buildup of magnetic twist before magnetar outbursts and a temporary spin-up (i.e., glitch) after releasing magnetic energy of the twisted fields by an outburst, as proposed in twisted-field magnetar models (e.g., Thompson et al. 2002; Beloborodov 2009; Carrasco et al. 2019). The observations are sparse, so we were not able to measure the evolution of the spin-down torque before and after the outburst. More detailed measurements of spin properties of magnetars near outburst epochs can help to improve the models further.

The pulse profiles in the earlier (seg. 1) and the later (seg. 2) data differ; the second peak is relatively larger and the separation between the peaks is smaller in the earlier ones (e.g., Fig. 2). While the change is not as dramatic as those seen after the 2006 (single to three peaks) or the 2011 (single to two peaks) outburst (e.g., Rodríguez Castillo et al. 2014), the change seems to be real as it can be seen by comparing individual observations with large statistics (e.g., *Chandra* data). The separation of the peaks in the first observation of seg. 2 (2 days before the 2018 outburst) is smaller $\Delta\phi = 0.20 \pm 0.03$ than those in the same segment but similar to those in seg. 1. This suggests that the change might have occurred near the outburst at MJD 58155. Moreover, emission (dominated by the low-energy band) of J1647 during the observation period is well described by a thermal model, and the size of the emitting region increased after the 2018 outburst (Borghese et al. 2019). Changes of magnetars’ emission properties after an outburst are expected in outburst relaxation models (e.g., Beloborodov 2013; Carrasco et al. 2019) which predict that emission at the stellar surface (the magnetic footprint on the star) could change after an outburst by bombardment of return currents in differently configured magnetic fields. However, the models are yet qualitative, and the statistics and cadence of the observations are not sufficient to measure the evolution of the temporal and spectral properties in details. Further theoretical works to make quantitative interpretation of spectral/temporal evolution and more observations near/after magnetar outbursts can help to understand mechanisms of outburst relaxation.

We estimated the magnetic-field strength of J1647 to be $\approx 4 \times 10^{13}$ G. Note that previous estimations of $|f|$ and so B_s ($\sim 10^{14}$ G; Israel et al. 2007; Woods et al. 2011; Rodríguez Castillo et al. 2014) are large but they may be biased by a putative glitch and its recovery at

the time as noted by Woods et al. (2011) and An et al. (2013). Although more data are needed to measure the true “baseline” B_s (e.g., without timing-noise effects), our measurements suggest that J1647 may add to the list of low-field magnetars. The source has shown at least five outbursts since the first one detected in 2006. The low dipole-field strength, large characteristic age and frequent activities suggest that multipole components should be strong in J1647 (e.g., Perna & Pons 2011; Viganò et al. 2013); its complex pulse profiles (1–3 peaks) previously observed after outbursts may be related to the multipole components. Or do magnetar outbursts cluster in time so that a magnetar is more likely to outburst over a certain period of time for a given long-term average outburst rate? Then, maybe we are observing clusters of outbursts of J1647 while its long-term average rate is actually very low for the low dipole field and large age. The low field strength and multiple outbursts make J1647 a particularly intriguing source for study of magnetar evolution, and future observational and theoretical works may give us new insights into magnetar physics.

We thank the anonymous referee for careful reading of the paper and insightful comments. This research was supported by Basic Science Research Program through the National Research Foundation of Korea (NRF) funded by the Ministry of Science, ICT & Future Planning (NRF-2017R1C1B2004566).

Facilities: NICER, NuSTAR, CXO, Swift

Software: HEASoft (v6.25; HEASARC 2014), CIAO (v4.10; Fruscione et al. 2006)

REFERENCES

- Alpar, M. A., Ertan, Ü., & Çalhşkan, Ş. 2011, *ApJL*, 732, L4
- An, H., Cumming, A., & Kaspi, V. M. 2018, *ApJ*, 859, 16
- An, H., Kaspi, V. M., Archibald, R., & Cumming, A. 2013, *ApJ*, 763, 82
- An, H., Kaspi, V. M., Beloborodov, A. M., et al. 2014, *ApJ*, 790, 60
- Archibald, R. F., Kaspi, V. M., Tendulkar, S. P., & Scholz, P. 2018, *ApJ*, 869, 180
- Archibald, R. F., Kaspi, V. M., Ng, C.-Y., et al. 2013, *Nature*, 497, 591
- Beloborodov, A. M. 2009, *ApJ*, 703, 1044
- . 2013, *ApJ*, 762, 13
- Borghese, A., Rea, N., Turolla, R., et al. 2019, *MNRAS*, 484, 2931
- Carrasco, F., Viganò, D., Palenzuela, C., & Pons, J. A. 2019, *MNRAS*, arXiv:1901.08889
- Clark, J. S., Negueruela, I., Crowther, P. A., & Goodwin, S. P. 2005, *A&A*, 434, 949
- de Jager, O. C., Raubenheimer, B. C., & Swanepoel, J. W. H. 1989, *A&A*, 221, 180
- Fruscione, A., McDowell, J. C., Allen, G. E., et al. 2006, in *Proc. SPIE*, Vol. 6270, Society of Photo-Optical Instrumentation Engineers (SPIE) Conference Series, 62701V

- Gavriil, F. P., Gonzalez, M. E., Gotthelf, E. V., et al. 2008, *Science*, 319, 1802
- Gendreau, K. C., Arzoumanian, Z., & Okajima, T. 2012, in *Proc. SPIE*, Vol. 8443, *Space Telescopes and Instrumentation 2012: Ultraviolet to Gamma Ray*, 844313
- Israel, G. L., Campana, S., Dall’Osso, S., et al. 2007, *ApJ*, 664, 448
- Kaspi, V. M., & Beloborodov, A. M. 2017, *ARA&A*, 55, 261
- Kuiper, L., Hermsen, W., den Hartog, P. R., & Collmar, W. 2006, *ApJ*, 645, 556
- Mereghetti, S., Pons, J. A., & Melatos, A. 2015, *SSRv*, 191, 315
- Muno, M. P., Clark, J. S., Crowther, P. A., et al. 2006, *ApJL*, 636, L41
- Olausen, S. A., & Kaspi, V. M. 2014, *ApJS*, 212, 6
- Perna, R., & Pons, J. A. 2011, *ApJL*, 727, L51
- Pons, J. A., & Rea, N. 2012, *ApJL*, 750, L6
- Rea, N., Esposito, P., Turolla, R., et al. 2010, *Science*, 330, 944
- Rodríguez Castillo, G. A., Israel, G. L., Esposito, P., et al. 2014, *MNRAS*, 441, 1305
- Scholz, P., Kaspi, V. M., & Cumming, A. 2014, *ApJ*, 786, 62
- Scholz, P., Camilo, F., Sarkissian, J., et al. 2017, *ApJ*, 841, 126
- Thompson, C., & Duncan, R. C. 1995, *MNRAS*, 275, 255
- . 1996, *ApJ*, 473, 322
- Thompson, C., Lyutikov, M., & Kulkarni, S. R. 2002, *ApJ*, 574, 332
- Tiengo, A., Esposito, P., Mereghetti, S., et al. 2013, *Nature*, 500, 312
- Turolla, R., Zane, S., Pons, J. A., Esposito, P., & Rea, N. 2011, *ApJ*, 740, 105
- Viganò, D., Rea, N., Pons, J. A., et al. 2013, *MNRAS*, 434, 123
- Woods, P. M., Kaspi, V. M., Gavriil, F. P., & Airhart, C. 2011, *ApJ*, 726, 37